ELSEVIER

International Journal of Mass Spectrometry 198 (2000) 189–211

International Journal of Mass Spectrometry

Studies on alkali and alkaline earth chromate by time-of-flight laser microprobe mass spectrometry and Fourier transform ion cyclotron resonance mass spectrometry. Part I: differentiation of chromate compounds

Frédéric Aubriet, Benoît Maunit, Jean-François Muller*

Laboratoire de Spectrométrie de Masse et de Chimie Laser, IPEM, Université de Metz, 1 Boulevard Arago, 57078 Metz, Cedex 03, France

Received 17 August 1999; accepted 9 February 2000

Abstract

Alkali and alkaline earth chromate compounds have been examined by time-of-flight laser microprobe mass spectrometry (TOF-LMMS) and laser ablation Fourier transform ion cyclotron resonance mass spectrometry (LA-FTICRMS). The two ion detection modes show a strong correlation with the nature of the counter ion. Similar behavior is observed with first alkali chromate and second alkaline earth chromate. In the positive detection mode, the major cluster ion induced by alkali chromate laser ablation is the $M_3CrO_4^+$ cation, whereas it refers to the two ion series $(MO)_nCrO^+$ and $(MO)_nCrO_2^+$ with $n = 1$–3 in the case of alkaline earth compounds. In the negative detection mode, whereas laser ablation of alkali chromate systematically produced mixed metal anions, in the case of alkaline earth chromate, such anions appeared but in small quantity and only in specific cases. The comparison of the results shown by FTICR mass spectra and TOF-LMMS allows for a distinction between stable and less stable ionic species, with the relative intensity of the latter dramatically decreasing on the FTICR mass spectra. Moreover, the decrease of the counter ion in electronegativity (radius growth) leads to an exacerbation of the typical behavior of the compounds belonging to the two ranges. These two observations facilitate the understanding of ion formation processes. This aspect of the study will be presented in Part II following the present work. (Int J Mass Spectrom 198 (2000) 189–211)

Keywords: Inorganic mass spectrometry; Laser ablation mass spectrometry; Mixed metal cluster ions; Chromium speciation; FTICRMS; TOFMS laser microprobe

1. Introduction

The toxicity of chromium compounds is closely dependent on its oxidation number. Whereas trivalent chromium is essential as a trace element for the ordinary life of living organisms (50–200 μg per day is necessary), hexavalent chromium is known to have toxic effects on biological systems [1]; it can in particular be a cause of DNA damage, cancer, or allergic reactions [2]. As a matter of fact, chromium VI is not genotoxic in itself, but its redox behavior produces species that are potentially toxic. The "uptake-reduction" model [1–3] clarifies the general mechanism of hexavalent chromium activity in the

* Corresponding author.

PII S1387-3806(00)00201-3

cellular and subcellular systems. This model postulates that chromium VI under physiological conditions (pH = 7.4) penetrates easily into cells, being transported by sulfates or phosphates, considering that the tetrahedral CrO_4^{2-} and pseudotetrahedal $HCrO_4^-$ ions have structural similarity with the biologically important inorganic anions SO_4^{2-} and PO_4^{3-}.

In cellular media, chromium compounds can produce cellular effects along two distinct pathways that are related though independent of each other.

The first one is an indirect pathway where hexavalent chromium undergoes intracellular reduction toward more stable trivalent species, producing reactive Cr (V) and Cr (IV) intermediates, simultaneously with the generation of reactive oxygen species (including H_2O_2, $HO^{\cdot}$, $^1O_2$, $O_2^{\cdot-}$, $ROO^{\cdot}$) and other free radical species. Hexavalent chromium reduction by glutathione generated both reactive Cr (V) and a glutathione–thiyl radical and caused direct damage in the form of glutathione–Cr–DNA complexes. In contrast to this glutathione reduction process, the reaction of Cr (VI) with H_2O_2 produced superoxide anion and/or hydroxyl radical, and led solely to breaks in the ROS-mediated DNA strand and 8-oxo-2′ deoxyguanosine [1–3].

The second pathway, by direct chromium III binding to DNA and/or nuclear proteins, consists mainly in DNA–DNA and DNA–protein cross-links and, to a lesser extent, in breaks in the single DNA strands [1–3]. Thus, the determination of chromium valence is of first importance from the point of view of health care and many techniques are used for the determination of the stoechiometry of chromium compounds. Two kinds of techniques can be identified.

The first group of techniques is well adapted to the analysis of liquid samples such as drinking, tap, ground, or sea water, and for the analysis of industrial waste water. However, when solubilization or preconcentration steps are required, these techniques are not convenient as they do not always provide the real ratio between Cr (III) and Cr (VI) in the sample. The most common techniques used are liquid UV/visible spectroscopy [4,5] or, to reduce interferences, in solid phase [6], atomic absorption spectroscopy [7], and electrochemical techniques [8,9]. The latter ones, on the basis of a original setup introduced by Turyan [10], make the detection of hexavalent chromium possible at a level as low as one part per trillion. To these standard techniques, we can add gas chromatography which, due to the formation of a volatile chelate, allows to establish amounts of hexavalent chromium at levels lower than a part per billion [11].

More recent developments allow both detection and quantification of the two (trivalent and hexavalent) chromium species without separation step. In particular, capillary electrophoretic techniques [12,13], ion chromatography analyses [14], high pressure liquid chromatography, combined with direct injection nebulization and inductively coupled plasma mass spectrometry [15], and reverse phase-high performance liquid chromatography coupled to various spectrometric detection methods [GF-AAS, inductively coupled plasma mass spectrometry (ICP-MS)] [16] make possible a simultaneous differentiation of the valence of chromium compounds. Frequently, standard techniques as common as atomic absorption spectroscopy are associated to original networks, allowing for on-line preconcentration and speciation of chromium compounds [17–19].

To overcome the problem of chromium valence ratio alteration by pretreatment operations, in situ techniques such as Raman [20,21] or x-ray absorption spectroscopy [22] [mostly x-ray absorption structure near edge structure (XANES) [23–25]] have been developed. These techniques require solid samples without pretreatment and provide, therefore, results that are more representative of chromium valence in the original sample. XANES investigations, in particular, allowed Bajt et al. to reach a detection limit of 10 ppm chromium (VI), with an accuracy of 5% in terms of Cr (VI)/total chromium [23]. However, this technique requires traditional synchrotron installations and cannot be used for routine work. Furthermore, the cost of experimentation is very high.

Another technique is mass spectrometry, coupled with a laser ablation/ionization process. Laser microprobe mass spectrometry (LMMS), coupled to a time-of-flight (TOF) or Fourier transform ion cyclotron resonance (FTICR) instrument [26,27] are used for the speciation of various oxidation numbers in different inorganic compounds. Consequently, these techniques have been used for investigation aiming at the speciation of iron [28,29], arsenic [30], titanium [31,32], lead [33], molybdenum [34], or copper [35] oxides.

Recently, Van Vaeck and co-workers [36–38] have published a series of papers bringing together the results provided by studies on various inorganic compound. In addition to differentiating different oxides with various stoechiometry, the distinction between (1) sulfates, sulfites, and thiosulfates and (2) nitrates and nitrites has been examined.

The determination of the valence of chromium by mass spectrometry has been the subject of some studies. Neubauer et al. [39] developed an on-line method allowing the speciation of chromium in aerosol particles by rapid single particle mass spectrometry. The distribution of ions in the negative detection mode provides a unique fingerprint of the chromium species. Stewart and Horlick [40] and Gwizdala et al. [41] have investigated the capacity of electrospray mass spectrometry (ESMS) to ensure the speciation of chromium (III) and chromium (VI). The formation of specific chromium ions [41], CrO_3^- for hexavalent chromium compounds, and $CrOCl_2^-$ for trivalent ones, allowed Gwizdala et al. to obtain differentiation with a detection limit of, respectively, 3 and 1.5 pg for Cr (III) and Cr (VI).

Considering the results obtained by static secondary ion mass spectrometry, Plog's model [42] allows, in particular, to have a differentiation between chromium compounds by a calculation of the ion fragment valence number. The relationship between ion intensity and the corresponding fragment valence number is specific to the original valence of the metal contained in the compound studied.

By transposing Plog's model to TOF-LMMS results, Poitevin et al. [43] developed a procedure based on the distribution of negative ion clusters to discriminate trivalent and hexavalent chromium compounds and allowing an identification of the stoechiometry of chromium in industrial dust particles with LAMMA instrument [20,43–45].

Our objective is to try and obtain a differentiation between trivalent and hexavalent chromium compounds using laser ablation Fourier transform ion cyclotron resonance mass spectrometry (LA-FTICRMS) and then proceed with TOF-LMMS studies. Furthermore, a better understanding of oxygenated cluster ions is important for a better selection of the criteria applied for speciation. This is the reason why our goal is also to establish the pathways for the formation of cluster ions occurring after irradiating the sample by laser.

For that purpose, we selected a range of trivalent and hexavalent chromium compounds including trivalent and hexavalent chromium oxides, trivalent chromium salt, chromite, and chromate compounds.

The first part of this study [46] investigated the capability of LA-FTICRMS and TOF-LMMS to speciate Cr_2O_3 and CrO_3 oxides. In this article, we intend to focus on the analysis of chromate compounds. Mass spectrometry analysis of trivalent compounds will be presented in a future publication.

In Part I of this study, we show the fingerprints of lithium, sodium, potassium, rubidium, cesium, magnesium, calcium, strontium, and barium chromate obtained by FTICRMS and TOF-LMMS investigations. As far as we know, it is the first ever presentation of a systematic study of alkali and alkaline earth chromate compounds by mass spectrometry.

Mass spectra in positive and negative ions display a similar behavior, on the one hand for alkali chromate and, on the other hand for alkaline earth chromate. A comparison of results obtained with LA-FTICRMS and TOF-LMMS enables us to make a distinction between stable and less stable species; it can be noticed that producing the latter type is smaller when LA-FTICRMS is used.

The results obtained allow us to identify the main parameters having an influence on the mechanism of cluster ion formation. The study of modifications on the fingerprint by experimental setup variations (power density, wavelength, and hydration degree) in Part II will make the investigation of the process of cluster ion formation possible.

2. Experimental

2.1. Chemicals

All commercial chemicals were of analytical reagent grade. Lithium chromate (94%) was purchased from Sigma (St. Louis, MO, USA); sodium nitrate (99%), chromium (VI) oxide (99%) from Aldrich (Milwaukee, WI, USA); potassium chromate (99.5%)

from Fluka (Buchs, Germany); rubidium, cesium, and calcium chromate with a purity of 99.9% from Cerac (Milwaukee, WI, USA), magnesium oxide (96%), strontium nitrate (99%), and barium nitrate (98.5%) from Prolabo (Paris, France).

2.2. Preparation of magnesium, strontium, and barium chromate

Magnesium chromate was prepared following Heinrich's method [47,48]. Small amounts of magnesia were added to an aqueous solution of hexavalent chromium oxide (42.3 g in 250 mL of de-ionized water) until reaching pH = 7. The solution was then filtered and cooled down at 0 °C. The water was removed at low pressure and at a temperature of 60 °C. We thus obtained a syrupy orange-colored solution. When immersed into an ice bath, the solution solidified and became lemon yellow in color. After filtration, the magnesium chromate was washed five times with ethanol (100 mL) and one time with 50 mL diethyl ether. The result was that 71.4 g of magnesium chromate pentahydrate $MgCrO_4$ $5H_2O$ was obtained (yield 73%).

Strontium and barium chromate were prepared following the procedure of, respectively, Authenrieth [49] and Schröder [50], by mixing separate aqueous solutions of sodium chromate and, respectively, strontium or barium nitrate. 250 mL of a near-saturation alkaline earth nitrate solution is mixed with 250 mL sodium chromate (40 g L^{-1}). The alkaline earth chromate was precipitated, filtered off on a Whatman filter paper (40 ashless), washed twice with 20 mL cold water and twice with 20 mL ethanol, dried at 120 °C in a furnace for 12 h and ground to a fine powder. 7.5 g of deep yellow strontium chromate $SrCrO_4$ (yield 23%) and 16.2 g of green-yellow barium chromate $BaCrO_4$ (yield 66%) were then obtained. Each of these compounds was controlled by x-ray diffraction; no impurities were detectable.

2.3. Instruments

2.3.1. Time-of-flight laser microprobe mass spectrometer

TOF-LMMS experiments were performed, using a LAMMA 500 instrument (Leybold-Heraeus, Germany) in a transmission arrangement. In our modified system [51,52], the second harmonic of a Nd-YAG laser (532 nm) pumps a dye laser (TDL 50D of Quantel, France) used for the ionization step. Harmonic frequencies of the dye laser are selected by a holographic network and can be doubled by a doubling crystal cell. A quartz separation prism separates the various wavelengths by adjusting its orientation. The laser beam selected can be aligned with a helium–neon pilot laser beam by adjusting the optical pathway.

The dye laser was calibrated by using a monochromator HR 320 with an average resolution, equipped with an interchangeable network, which allowed us to scan the UV wavelengths.

We selected a resonant wavelength of chromium at 357.9 nm to enhance the production of Cr^+ ions [46]. The assignment of resonance in the photoionization process is $A[\omega_1, \omega_1 e^-]A^+$. Two photons of the same laser pulse are absorbed successively by the chromium atom—produced by ablation of the analyte performed by the first photons of the laser pulse—in the laser plume. The former photon allows $^7S_3 \rightarrow {}^5P_4$ transition and the latter brings the excited chromium atom to its ionization continuum.

The LDS 698 exciton dye allowed us to obtain laser wavelengths ranging from 670 to 730 nm; wavelengths in the range 335–365 nm were obtained by using a K_2DPO_4 doubling crystal (λ = 357.9 nm, pulse duration 12 ns, output energy used 0.2–0.8 mJ). In all cases, the power density used was 3×10^7 W/cm^2. All spectra were recorded on a Nicolet Pro50 transit recorder (Madison, WI, USA).

2.3.2. Laser microprobe Fourier transform ion cyclotron resonance mass spectrometer

These analyses were performed using a laser microprobe FTICR mass spectrometer that has been described in detail elsewhere [53,54]. This instrument is a modified differentially pumped, dual-cell Nicolet Instrument FTMS 2000 (Finnigan FT/MS, now named ThermoQuest, Madison, WI, USA) operated with a 3.04 T magnetic field and coupled to a reflection laser interface.

The viewing system, using an inverted Cassegrain

optics design, allows the visualization of the sample with 300-fold magnification. A new sample probe fitted with motorized micromanipulators into the three spatial directions permits attainment of a spatial accuracy of less than 10 μm.

The ionization step was performed using the third harmonic of a Nd-YAG laser (λ = 355 nm, pulse duration 4.3 ns, output energy used 0.8 mJ). Alternatively, an excimer laser charged with an ArF mixture (λ = 193 nm, pulse duration 23 ns, output energy 1.6 mJ) was used. The diameter of the laser beam on the sample (placed inside the source cell) can be adjusted by means of the internal lenses and an external adjustable telescope from five to several hundred micrometers, which corresponds to a power density ranging from 10^{10} to 10^{6} W/cm^2.

The experiment sequence used for these analyses is as described: ions are formed by laser ablation in the source cell (residual pressure less than 10^{-6} Pa). During the ionization event, the conductance limit plate between the two cells and the source trap plate are kept at a trapping potential of typically 2 V (respectively, -2 V in the negative detection mode) or a lower potential in some particular cases (down to 0.25 V). A variable delay period follows, during which ion/molecule reactions can occur. Ions are then excited by a frequency excitation chirp and the resulting image current is detected, amplified, digitized, apodized (Blackman-Harris, three terms), and Fourier transformed to produce a mass spectrum.

Note that all experiments were performed with a Cr^+ and M^+ ejection [46] (where M is the counter ion of the chromate compounds) in order to enhance the detection of the signal delivered by mixed oxygenated cluster ions. In fact, all atomic ions are likely to induce a dissociation of cluster ions by collision and therefore disturb the detection of the latter. Indeed, the (partial or total) ejection of the large majority of atomic ions allows an increase in the potentiality to detect them, and this without any loss of information, at least in the conditions of our investigation. Each FTICR mass spectrum resulted from an average of 100 laser shots fired on consecutive spots.

Ion assignment is performed by measuring the exact mass, after calibrating and identifying the isotopic distribution.

3. Results and discussion

3.1. Foreword

In our discussion, we often refer to the electronegativity of alkali and alkaline earth compounds, and their affinity with oxygen. Affinity to oxygen may be related to MO gaseous enthalpy of formation (M = Li, Na, K, Rb, Cs, Mg, Ca, Sr, Ba, or Cr). Table 1 presents (1) the Pauling and Sanderson electronegativity for alkali, alkaline earth, and chromium—we added the corresponding figures for oxygen—and (2) the MO gaseous enthalpy of formation for the same metals at 298 K.

3.2. Analysis of alkali chromate compounds in positive ion detection mode

3.2.1. TOF LMMS studies

The positive time-of-flight laser microprobe mass spectra of lithium, sodium, potassium, rubidium, and cesium chromate (Fig. 1) showed ions which may be expressed by the general formula $M_nCr_xO_y^+$ (n = 1–5; x = 0–3; and y = 0–9). In fact, the ions induced by laser ablation/ionization of alkali chromate compounds can be classified in three cluster ion groups.

The first one contained cluster ions with only oxygen and alkali atoms; some hydrogen atom adducts may occur. The more representative ion of the latter type is the cluster ion M_2OH^+, where M = Li, Na, K, Rb, or Cs.

Mixed metal ions, which contained oxygen, alkali, and chromium atoms constitute the second and third clusters ion groups.

The first series of mixed metal cluster ions, with only one chromium atom, have in all cases the highest relative intensity. They may be expressed by the general formula $(MO)_nCr^+$ and $(MO)_nCrO^+$ (n = 2, 3, or 4). This ionic expression does not want to reflect the general process of ion formation, but it provide a

Table 1
Pauling and Sanderson electronegativity of alkali and alkaline earth compounds; enthalpy of MO (g) formation at 298 K

Compound	Pauling electronegativity[a]	Sanderson electronegativity[b]	Enthalpy of MO (g) formation, in kJ/mol at 298 K[c]
Lithium	0.98	0.89	84.10
Sodium	0.93	0.56	83.68
Potassium	0.82	0.45	71.13
Rubidium	0.82	0.31	n.d.[d]
Cesium	0.79	0.22	62.76
Magnesium	1.31	1.32	58.15
Calcium	1.00	0.95	43.93
Strontium	0.95	0.72	−13.39
Barium	0.89	0.68	−123.80
Chromium	1.66	1.66	188.28[e]
Oxygen	3.44	3.65	. . .

[a] Data from [65].
[b] Data from [66].
[c] Data from [67].
[d] No data found.
[e] Enthalpy of CrO_2 and CrO_3 formation at 298 K are, respectively, equal to −75.31 and −292.88 kJ/mol (from [67]).

satisfying account of the nature of the first series of mixed metal cluster ions produced by an ablation/ionization of alkali chromate compounds.

The most intense cluster ions in this series are in all cases the $M_3CrO_4^+$ ions. This mixed series of metal cluster ions, contrary to the following ones, has already be observed in previous studies of sodium and potassium chromate [20,43,44,55].

The second type of mixed metal cluster ions consists of structures with two or three chromium atoms. The more intense ions in this series are the two structures $M_4Cr_2O_6^+$ and $M_5Cr_2O_8^+$, except in the study of the potassium chromate compound [Fig. 1(b)] where only the first one is detected with reasonable intensity, the second one (not shown) is in very small abundance.

These ions are well described by the general formulae $(CrO_2)_m(MO)_nCrO_x^+$ where $m = 1$ or 2, $n = 3$–5, and $x = 0$ or 1.

3.2.2. FTICRMS studies

The positive FTICR mass spectra obtained with alkali chromate (Fig. 2) confirmed the TOF-LMMS studies. It could be verified that all these compounds display a similar behavior, with the FTICR mass spectrum obtained for each chromate showing many similarities with the spectra provided by the other chromate.

Identical ions, except for alkali-oxygen ions, are observed when using the two mass spectrometric techniques. However, relatively large differences are revealed by a comparison between fingerprints supplied by FTICRMS and TOF-LMMS. The most characteristic difference is a significant increase in the relative intensity of $M_3CrO_4^+$. Except for the fingerprint of lithium chromate, the relative intensity of the other cluster ions represents only a very low percentage of the former.

By comparing the relative intensity of the $M_3CrO_4^+$ cluster ions to that of other cluster ions, we can observe that the relative intensity of the former increases as the alkali radius also grows. At the same time, the number of mixed cluster ions decreases: 13 for lithium chromate [Fig. 2(a)], and 7 for rubidium and cesium chromate [Figs. 2(d) and 2(e), respectively]. Moreover, the cluster ions with more than one chromium atom in their structure display a dramatic decrease. The corresponding number drops from 7 to 2 when lithium and cesium chromate are studied [Figs. 2(a) and 2(e), respectively].

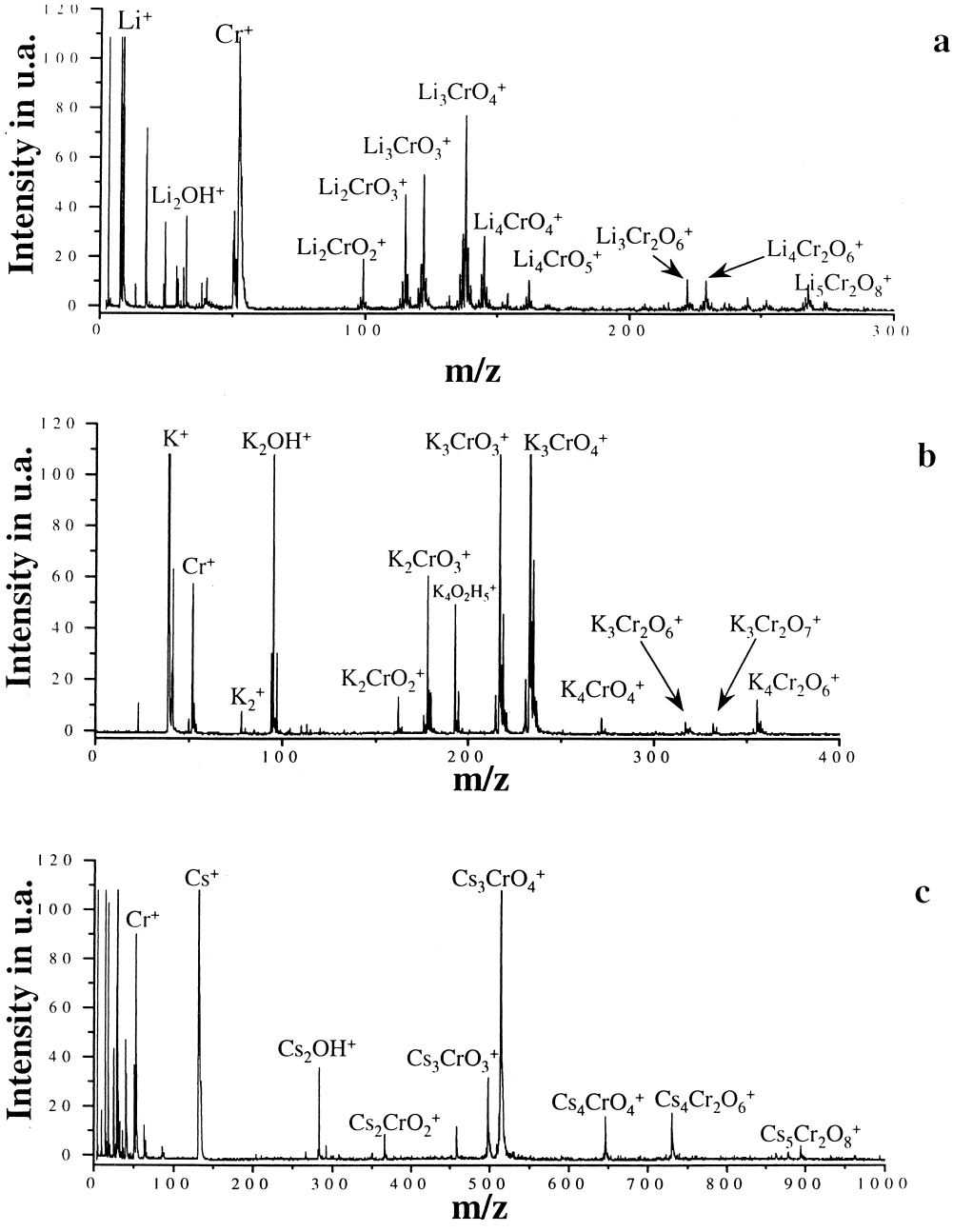

Fig. 1. Positive TOF-LMMS fingerprints of (a) Li_2CrO_4, (b) K_2CrO_4, and (c) Cs_2CrO_4 at a wavelength of 357.87 nm, with a power density of 3×10^7 W/cm^2.

These observations should be correlated to a decrease in electronegativity observed for the alkali atom, which implies an increasing affinity with the oxygen atom (Table 1).

Figure 2(a) shows a mass spectrum obtained typically when investigating lithium chromate by LA-FTICRMS. The $^6Li^+$ and $^7Li^+$ ions appear at *m/z* values of, respectively, 204.889 and 35.042. Both ions

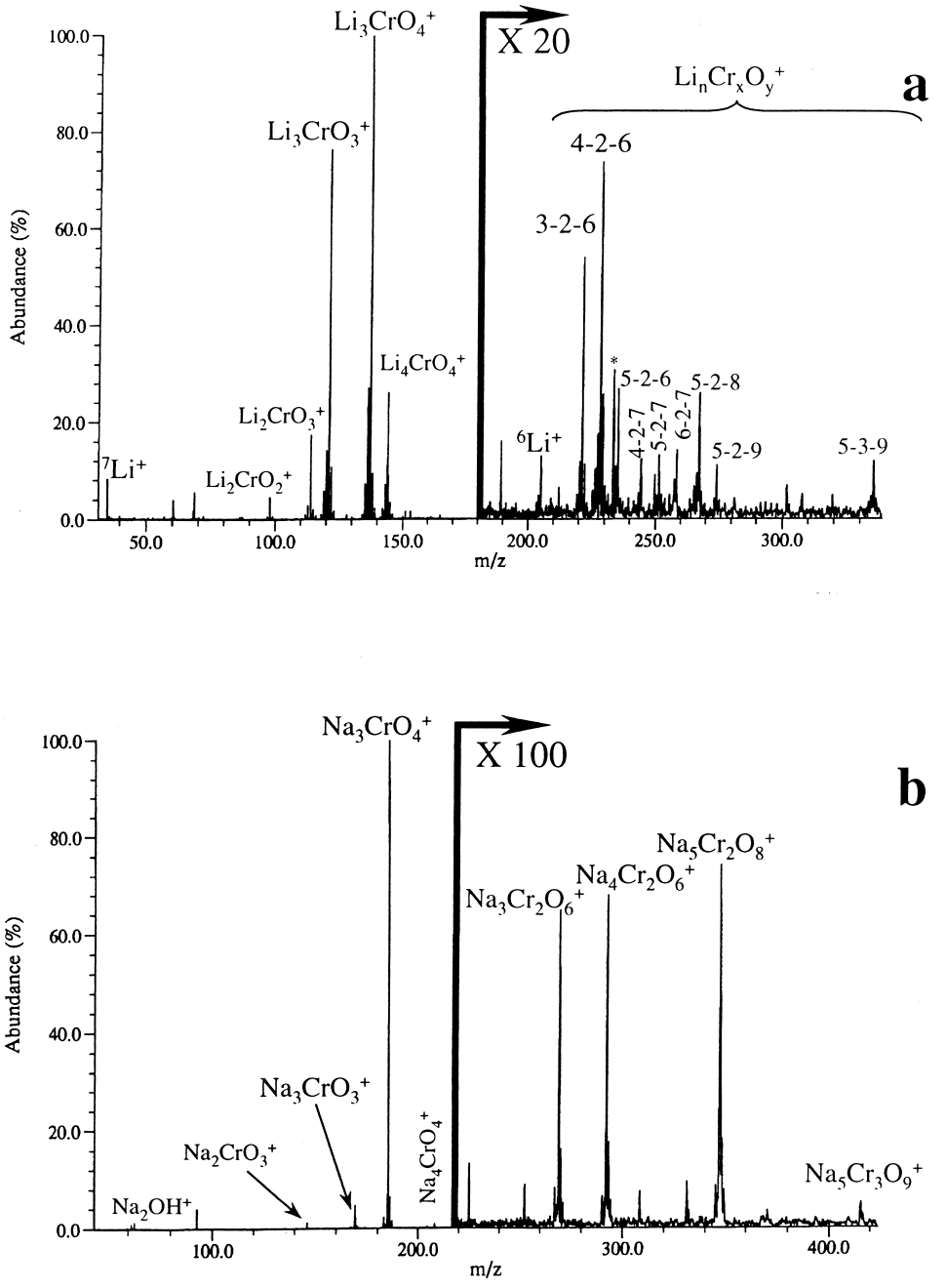

Fig. 2. Positive LA-FTICRMS fingerprints of (a) Li_2CrO_4, (b) Na_2CrO_4, (c) K_2CrO_4, (d) Rb_2CrO_4, and (d) Cs_2CrO_4 at wavelength 355 nm, with a power density in the range 10^7–10^8 W/cm^2. The ion indexed (asterisk) on the lithium chromate spectrum (a) is an electronic artifact. The interpretation of the ions at *m/z* 419, 421, and 423 on the fingerprint (d) of rubidium chromate is pending; however, their presence can seemingly be assigned to some impurity of the chromate compound.

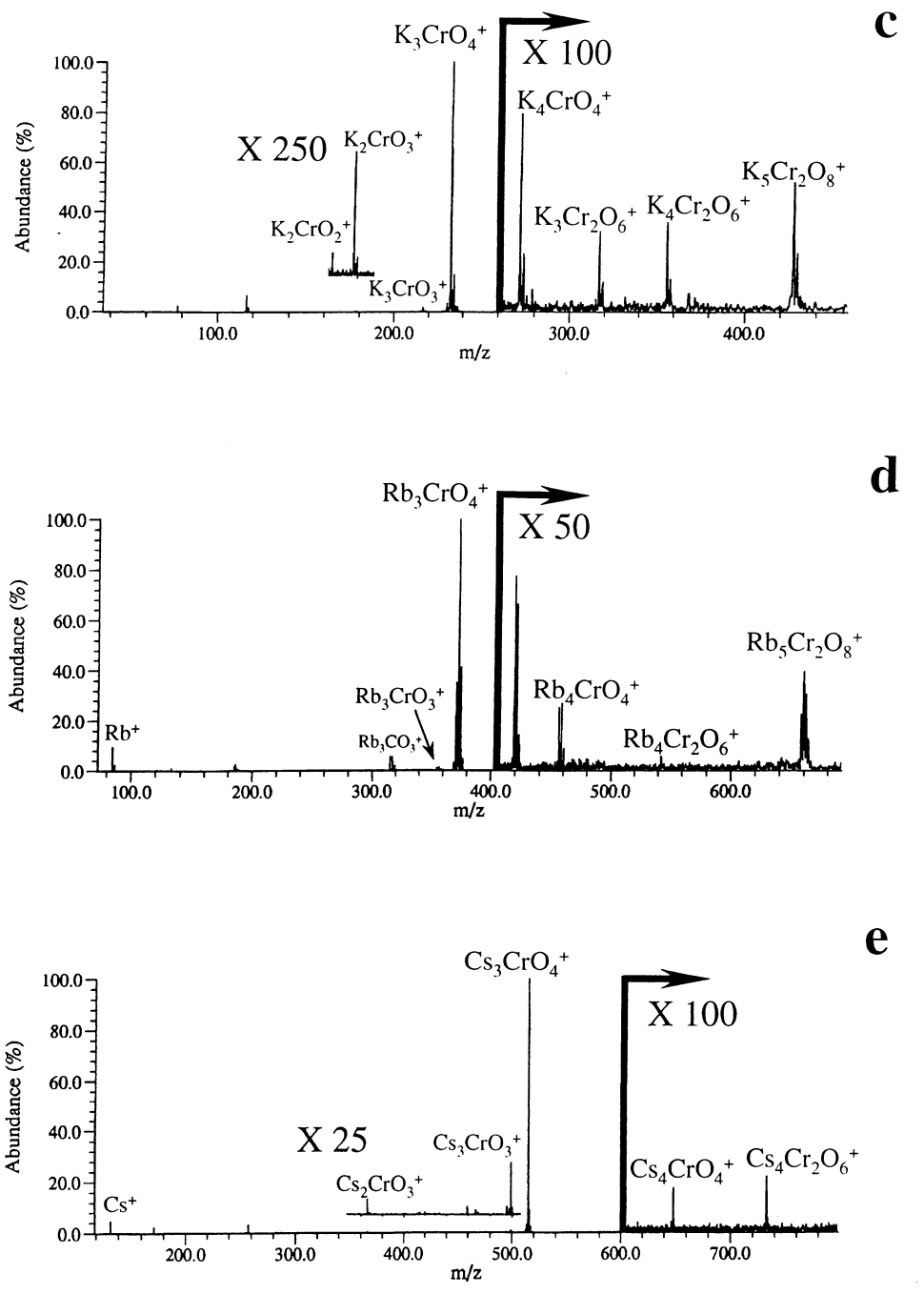

Fig. 2. (Continued)

undergo foldover. In fact, with a 3.04 tesla magnetic field, ions with a *m/z* value lower than 18 are submitted to the foldover effect as they do not respect the Nyquist criterion. These ions appear on the mass spectrum at frequency corresponding, respectively, to an arrangement of the cyclotronic frequency with the frequency acquisition rate [56].

As a preliminary conclusion, we may say that

TOF-LMMS and LA-FTICRMS studies of alkali chromate enhance the stability of the $M_3CrO_4^+$ structure. In fact, the particular design of the FTICRMS instrument accounts for the relative stability of the cluster ions induced by laser ablation/ionization. The time interval between the laser shot—inducing the formation of the ions—and the detection of ions could possibly permit a dissociation of less stable ions. The separation observed between TOF-LMMS and FT-ICRMS mass spectra can be taken as a possible means to reveal the relative stability of the various mixed cluster ions trapped in the FTICR cell.

3.3. Analysis of alkali chromate compounds in negative ion detection mode

3.3.1. TOF LMMS studies

The mass spectra obtained in negative mode with alkali chromate (Fig. 3) betray—just as in the positive detection mode—that these compounds behave in a similar way when they are laser ablated.

Two types of cluster ions are observed on mass spectra: the first series is made up of $Cr_xO_y^-$ ions, with $x = 1–3$ and y = 2–9.

Contrary to what was observed with the distribution of first-generation oxygen chromium ions, where the intensity of the CrO_2^- ion is always lower than that of CrO_3^-, differences appear in the distribution of the second-generation ($x = 2$) oxygen chromium cluster ions. Although the intensity of $Cr_2O_4^-$, $Cr_2O_5^-$, and $Cr_2O_6^-$ increases in this order on the negative mass spectrum of lithium chromate [Fig. 3(a)], this distribution profile displays the opposite tendency when cesium chromate is under study [Fig. 3(c)]. This development may be, as in the positive detection mode, assigned to the increasing affinity of the oxygen alkali, as compared to that of chromium oxygen (Table 1).

The second series consists of mixed metal cluster ions; these are proper to the compound studied. Their structure corresponds to the general formula $M_nCr_xO_y^-$, with $n = 1–3$, $x = 1–3$, and $y = 4–9$. It should be noted that the highest amount of mixed metal ions was obtained when investigating the most electronegative alkali compounds.

3.3.2. FTICRMS studies

As in the case of TOF-LMMS spectra, two kinds of ions can be detected by FTICRMS after laser ablation/ionization of chromate compounds (Fig. 4). The first one is chromium oxygen cluster anions, such as $Cr_xO_y^-$, and the second one is mixed metal oxygenated cluster ions $M_nCr_xO_y^-$.

Moreover, when investigating alkali chromate by TOF-LMMS note that the negative $M_nCr_xO_y^-$ ions have weak intensity, corresponding to a small percentage of the intensity of $Cr_xO_y^-$ cluster ions.

Most ions displayed on TOF-LMMS alkali chromate mass spectra are still detected by the FTICR mass spectrometer, but we observe important variations in relative intensity. For instance, the relative intensity of the CrO_2^- cluster ion decreases strongly when FTICRMS results are compared to those supplied by TOF-LMMS. This observation could be accounted for by the assumptions concerning stability that were put forward to justify a similar behavior in the positive detection mode (e.g. the relative intensity of $M_3CrO_4^+$ increasing on FTICR mass spectra). The low representation of CrO_2^- cluster ions on FTICR mass spectra may be accounted for by its lower stability level as compared to that of CrO_3^- [55].

Another illustration is the development of the relative intensity of $Cr_2O_4^-$, $Cr_2O_5^-$, and $Cr_2O_6^-$: which stays unchanged in the FTICRMS experiments for the five alkali chromate, as opposed to the TOF-LMMS fingerprints.

Moreover, the number of ions on the negative fingerprint and the relative intensity of $Cr_2O_y^-$ ions decrease when the radius of alkali atoms increases. At a power density of 5×10^7 W/cm^2 (Table 2), the less electronegative the alkali atoms are, the less numerous the mixed metal anions (14 for Li_2CrO_4 and only 3 for Cs_2CrO_4) are detected.

This development could likewise be assigned to the affinity of alkali oxygen (Table 1), which increases as the electronegativity of alkali atoms decreases (and the radius increases). Therefore, the difference in electronegativity between chromium and alkali compounds, in increasing order with lithium, sodium, potassium, rubidium, and cesium chromate, could account for the decrease in the production of

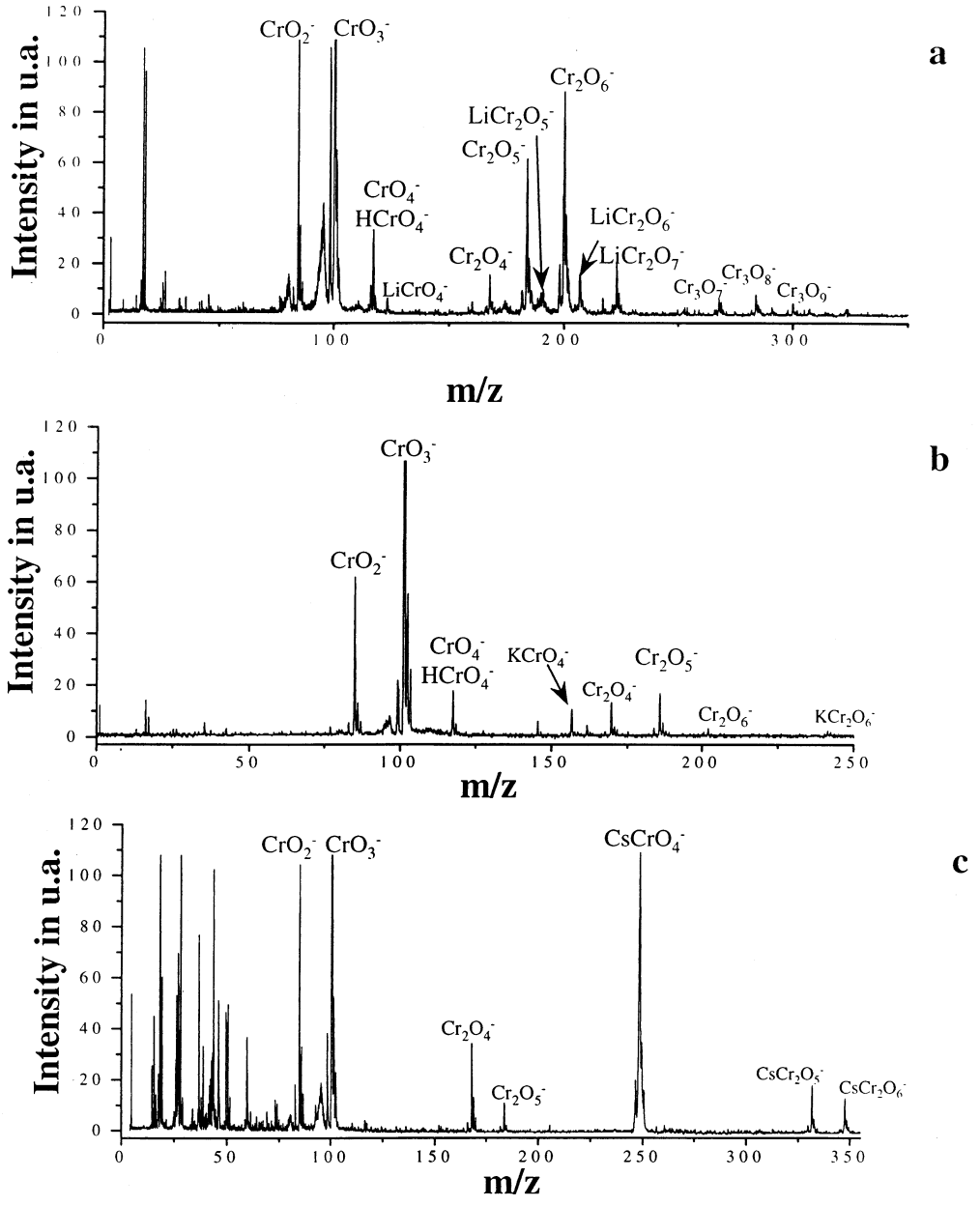

Fig. 3. Negative TOF-LMMS fingerprints of (a) Li_2CrO_4, (b) K_2CrO_4, and (c) Cs_2CrO_4 at a wavelength of 357.87 nm, with a power density of 3×10^7 W/cm^2.

$Cr_xO_y^-$ species in the plume, whereas the production of oxygen alkali species increases. Furthermore, we may also relate this development to the increase in relative abundance observed with $MCrO_4^-$, $MCr_2O_6^-$, and $MCr_2O_7^-$ when the five alkali chromate are successively studied by FTICRMS. The higher yield obtained with these three ionic structures may restrict the production of other oxygenated anions.

More generally, it appears that the higher the difference in electronegativity between chromium and

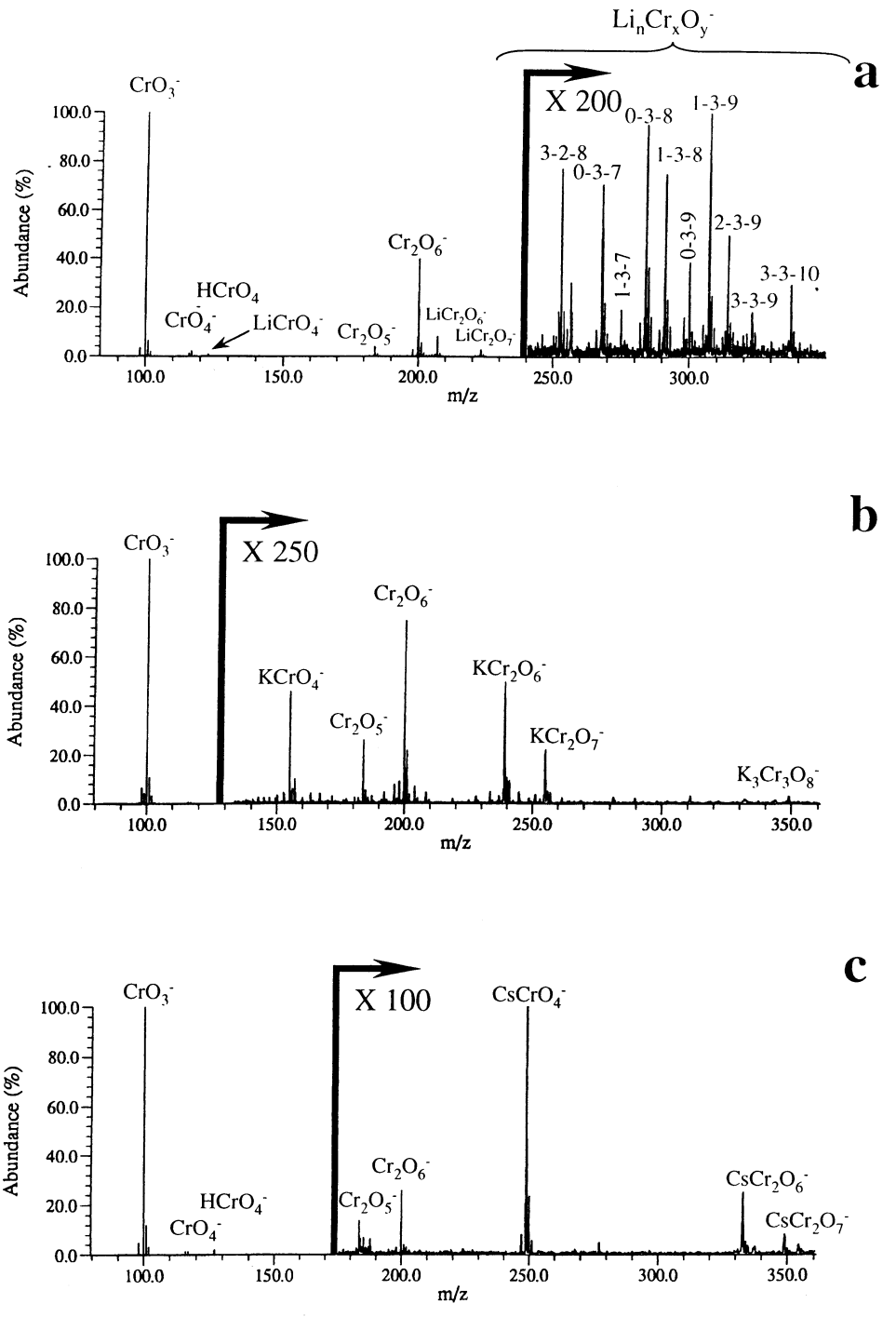

Fig. 4. Negative LA-FTICRMS fingerprints of (a) Li_2CrO_4, (b) K_2CrO_4, and (c) Cs_2CrO_4 at a wavelength of 355 nm, with a power density in the 10^7–10^8 W/cm^2 range.

Table 2
Relative distribution of mixed cluster anions on the fingerprint of alkali chromate compounds, obtained at 355 nm with the same FTICRMS experimental sequence and at a power density of 5×10^7 W/cm^2 in the study of Li_2CrO_4, Na_2CrO_4, K_2CrO_4, Rb_2CrO_4, and Cs_2CrO_4[a]

	Compounds				
Cluster ions	Li_2CrO_4	Na_2CrO_4	K_2CrO_4	Rb_2CrO_4	Cs_2CrO_4
$MCrO_4^-$	0.111 ± 0.031	0.049 ± 0.005	0.456 ± 0.042	0.392 ± 0.062	0.811 ± 0.082
$MCr_2O_5^-$	0.091 ± 0.016	...	...	...	...
$MCr_2O_6^-$	0.511 ± 0.054	0.668 ± 0.027	0.319 ± 0.033	0.402 ± 0.033	0.135 ± 0.068
$MCr_2O_7^-$	0.131 ± 0.046	0.177 ± 0.024	0.198 ± 0.015	0.073 ± 0.033	0.054 ± 0.016
$MCr_3O_7^-$	0.026 ± 0.008	...	...	...	...
$MCr_3O_8^-$	0.026 ± 0.007	0.014 ± 0.002	...	...	...
$MCr_3O_9^-$	0.013 ± 0.005	...	...	...	...
$M_2Cr_2O_7^-$	...	0.008 ± 0.001	...	...	...
$M_2Cr_3O_8^-$	0.021 ± 0.006	...	...	...	...
$M_2Cr_3O_9^-$	0.019 ± 0.008	0.012 ± 0.005	...	...	...
$M_3Cr_2O_8^-$	0.028 ± 0.007	0.059 ± 0.008	0.028 ± 0.009	0.132 ± 0.038	...
$M_3Cr_3O_9^-$	0.010 ± 0.006	...	...	...	...
$M_3Cr_3O_{10}^-$	0.012 ± 0.005	0.015 ± 0.006	...	...	...

[a] The value mentioned first corresponds to the ratio between the absolute intensity of the cluster ions specified and the sum of absolute intensities for all mixed metal oxygenated cluster anions $M_xCr_yO_z^-$. The second one is the relative standard deviation computed after twenty FTICRMS experiments (each experiment consists in establishing an average after 100 laser shots onto consecutive spots).

alkali atoms, the more intense the positive cluster ions—including alkali atoms—and the less intense the negative oxygenated chromium ions were.

Moreover, the higher number and intensity of mixed metal anions in the negative detection mode and cluster cations with only one chromium atom when the alkali atom radius increases may be correlated with the counter ion polarizability (Table 3). Being more polarizable, the largest alkali atoms induce oxygenated neutral species, in particular MO ones, which have a greater dipole moment. Due to this, their affinity with the positively charged chromium atom increases with the increase in radius of the alkali atom.

Jöst et al. [57], on the basis of TOF-LMMS studies of a NaCl–CsCl mixture at a 1000:1 molar concentration, showed that the clusters observed as being in a majority belong to the fingerprint of cesium chloride. It appears experimentally that the greater the difference in electronegativity between the halogen atom and the alkali one, the more efficient the ion formation process was. The results obtained with alkali chromate compounds by FTICRMS systematic study are consequently consistent with the work

Table 3
Polarizability of alkali and alkaline earth compounds

Compound	Polarizability[a,b]	Compound	Polarizability[a,b]
Lithium	24.3[c]	Magnesium	10.6[c]
Sodium	23.6[c]	Calcium	22.8[c]
Potassium	43.4[c]	Strontium	27.6[d]
Rubidium	47.3[c]	Barium	39.7[d]
Cesium	59.3[c]	Oxygen	0.802[c]

[a] Data from [68].
[b] Expressed in units of 10^{-24} cm^3.
[c] Accuracy ±2%.
[d] Accuracy ±8%.

performed by Jöst et al. [57] on alkali halides and with the experimental studies recently carried out by ESMS techniques [58]. The latter showed experimentally that, in the homologous alkali halide series, the relative abundance of cluster ions increased with the increasing size of the cation in positive detection mode and the anion in negative detection mode.

3.4. Analysis of alkaline earth chromate compounds in positive ion detection mode

3.4.1. TOF LMMS studies

Four alkaline earth chromate—magnesium, calcium, strontium, and barium compounds—have been examined successively. To ensure easier comparison, pentahydrated magnesium chromate was heated up to 200 °C for 24 h to remove crystalline lattice water [59]. The importance of lattice water in relation to the fingerprint obtained will be investigated in the second part of this work and we try to demonstrate the importance of lattice water on the pathways of cluster ion formation.

One can notice that two kinds of ions are systematically present on the fingerprints obtained by TOF-LMMS for alkaline earth chromate compounds (Fig. 5).

The first group of cluster ions observed when investigating alkaline earth oxides, nitrates, and carbonates [60–62] showed, on one hand, substoechiometric $(MO)_nM^+$ ions and, on the other hand, stoechiometric $(MO)_n^+$ ions. Moreover, protonated $(MO)_nH^+$ were also detected. The latter had been observed previously in the systematic investigation of alkaline earth nitrate compounds by mass spectrometry [62]. Depending on the radius of the alkaline earth atom M, the number n ranges from 0 to 4.

As when studying the alkali chromate, the mixed metal cluster ions that make up the second series could be subdivided into two groups, depending on whether they displayed one or two chromium atoms in their structure.

In the first group, $(MO)_nCrO^+$ and $(MO)_nCrO_2^+$ ions ($n = 1$–4) were observed; they had been obtained in previous studies [20,43,44,55]. As for the second one, it is composed in $(MO)_n(CrO_2)CrO_x^+$ and $(MO)_n(CrO_3)CrO_x^+$ ions, where $x = 1$ or 2 and $n = 1$ or 3. Note that the smaller the atomic radius of the alkaline earth, the smaller the first n number in the series. We may refer to the increase in polarizability of the counter ion as the radius increases (see the case in alkaline chromate studies) to account for the greater importance of cluster ions containing only one chromium atom in their structure.

The similarity in behavior for the set of alkaline earth chromate is remarkable, considering that the same cluster ions are always present. However, some differences appear when we compare the relative distribution of $(MO)_nCrO^+$ and $(MO)_nCrO_2^+$ ions. For $n = 1$, when the magnesium [Fig. 5(a)] and calcium chromate are studied by TOF-LMMS, the $(MO)CrO^+$ cluster ion is always the most intense. As opposed to this, with strontium and barium [Fig. 5(b)] chromate the $(MO)CrO_2^+$ ion represents the greatest cluster ion. When the number n increases, similar profiles in the distribution of the $(MO)_nCrO^+$ and $(MO)_nCrO_2^+$ ions are observed. $(MO)_nCrO_2^+$ cation is always the most intense cluster ion, whatever the alkaline earth chromate.

3.4.2. FTICRMS studies

A comparison of the mass spectra obtained by the two mass spectrometry techniques showed a slight decrease of the oxygenated alkaline earth cluster ions to the benefit of the mixed metal oxygen cluster ions on the FTICR mass spectra. The larger the radius of the alkaline earth, the larger this benefit was (Fig. 6). Concerning the other ions, the mass spectra obtained in the study of alkaline earth chromate by FTICRMS are almost the same as those observed when these compounds were analyzed by TOF-LMMS. Only small changes in intensity and in the appearance/disappearance of some low-quantity cluster ions could be noted.

Nevertheless, when magnesium chromate was investigated [Figs. 5(a) and 6(a)], a third ion group appeared composed of pure oxygenated chromium cluster ions. Cr_2O^+, $Cr_2O_2^+$, and $Cr_2O_3^+$ ions are well identified on the FTICR fingerprint of magnesium chromate. Moreover, the lower signal/noise ratio observed on the magnesium chromate fingerprint [Fig.

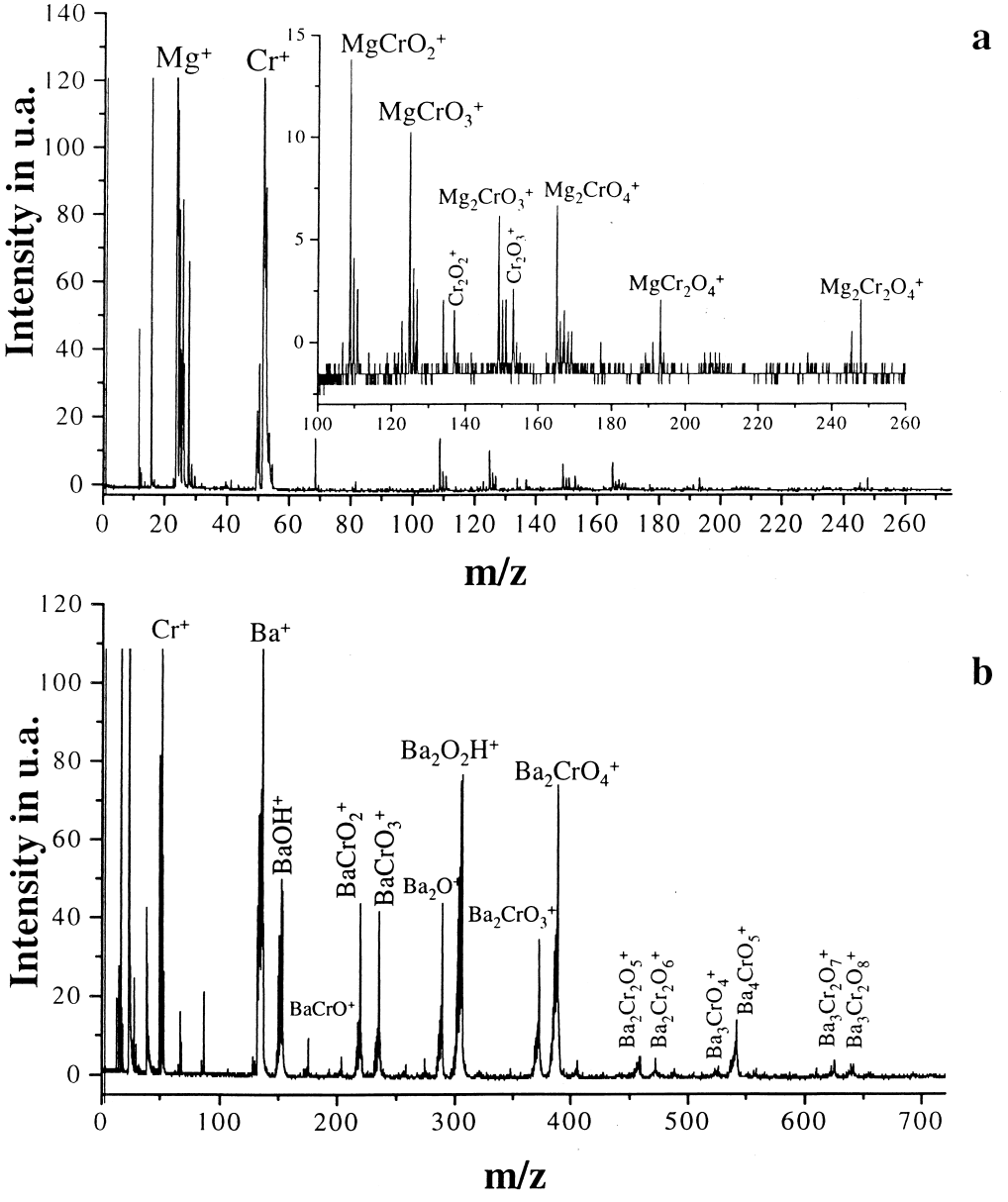

Fig. 5. Positive TOF-LMMS fingerprints of (a) $MgCrO_4$ and (b) $BaCrO_4$ at a wavelength of 357.87 nm, with a power density of 3×10^7 W/cm^2.

6(a)] seems to indicate a smaller production of mixed metal cluster ions after laser irradiation of this compound. Furthermore, the strong CrO^+ ion signal (*m/z* 68) proves a decrease of magnesium species and an increase of chromium species in the laser plume, as compared to what was observed with the other earth alkali chromate. The weaker sensitivity and the presence of an important noise on the TOF laser microprobe mass spectra could account for the fact that most ions present on the FTICR magnesium chromate fingerprint [Fig. 6(a)] were not observed when the TOF-LMMS studies were conducted [Fig. 5(a)].

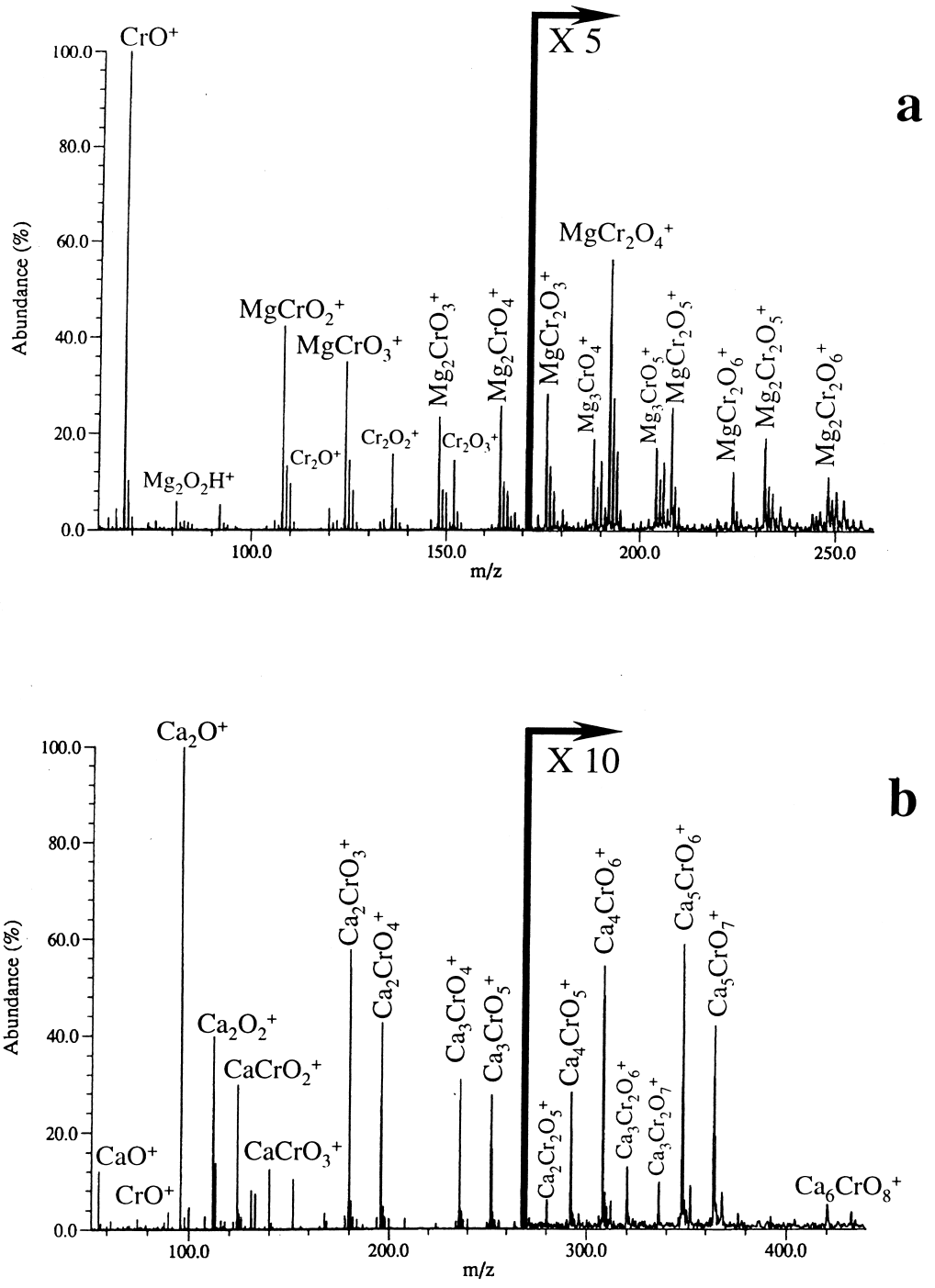

Fig. 6. Positive LA-FTICRMS of (a) $MgCrO_4$, (b) $CaCrO_4$, (c) $SrCrO_4$, and (d) $BaCrO_4$ chromate compounds at a wavelength of 355 nm, with a power density in the 10^7–5×10^8 W/cm^2 range.

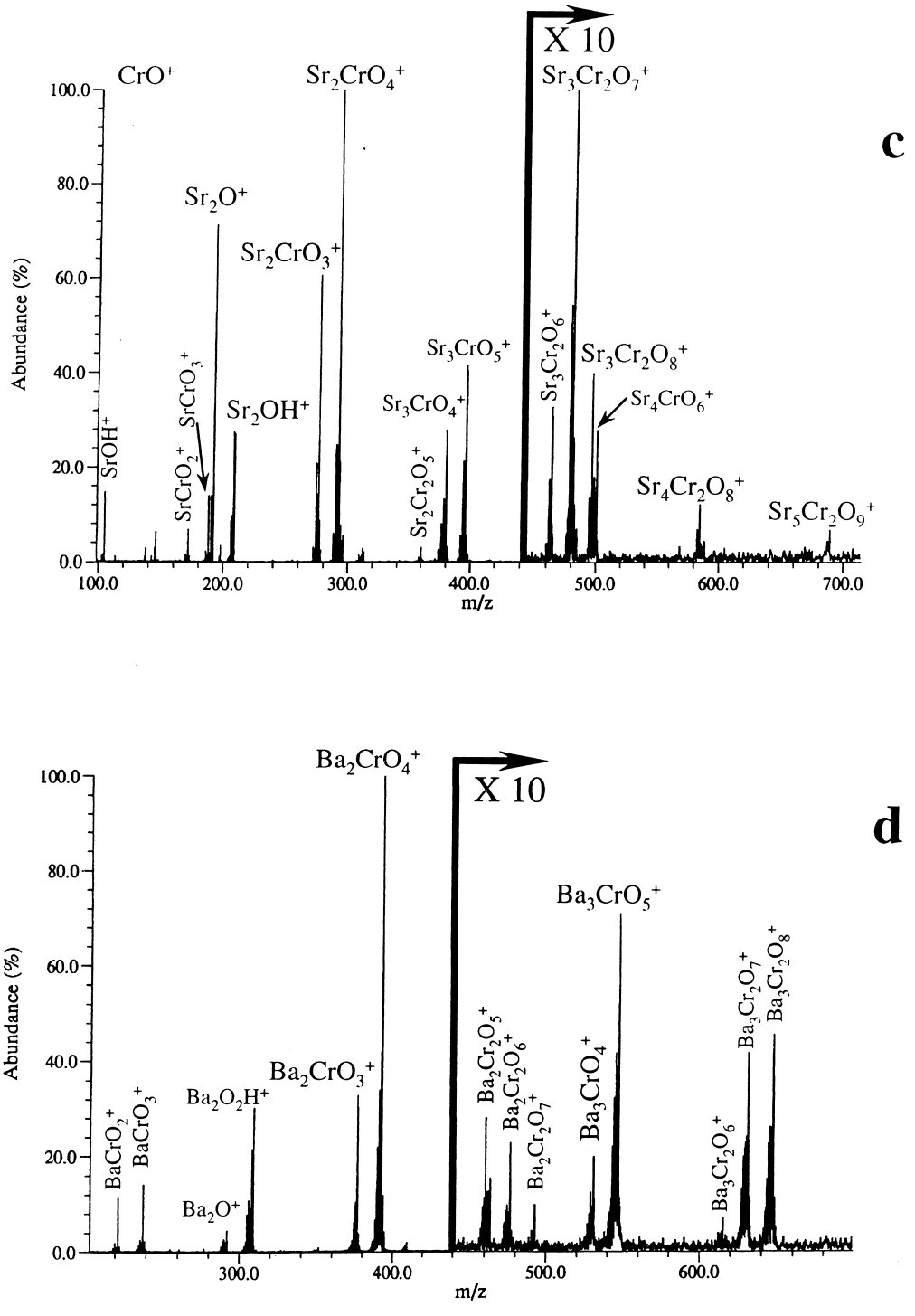

Fig. 6. Continued

Whereas no oxygenated chromium cluster ions were detected with the calcium, strontium and barium [Fig. 6(b)] compounds, three of them appeared on the FTICR mass spectrum of magnesium chromate. The difference in electronegativity between chromium and alkaline earth compounds may account for this development. In fact, the difference in electronegativity between oxygen and, respectively, calcium, strontium, and barium increases in this order though values remains close to one another, whereas this difference between oxygen and magnesium is weaker and is close to that of oxygen chromium (Table 1).

Thus, we may account for the presence of oxygenated chromium on the fingerprint of positive ion magnesium chromate. Moreover, a low difference in affinity for chromium and magnesium oxygen offers the possibility of producing more easily oxygenated chromium species in the plume after laser ablation. Being more present, such species have a growing importance in the process of ion formation; in particular (1) pure oxygen chromium cluster ions are present and (2) the mixed metal ions with more than one chromium atom $(MO)_n(CrO_2)CrO_x^+$ and $(MO)_n(CrO_3)CrO_x^+$ ($x = 1$ or 2) appear earlier, with a lower n value ($n = 1$), compared to the results obtained with calcium, strontium and barium chromate.

3.5. Analysis of alkaline earth chromate compounds in negative ion detection mode

3.5.1. TOF LMMS studies

As when studying alkali chromate in the negative detection mode by TOF-LMMS (Fig. 7), the most important ions observed were pure oxygenated chromium cluster ions $Cr_xO_y^-$ ($x = 1$ or 2, $y = 1$–6). Some low-quantity mixed metal ions were obtained after laser irradiation of magnesium and barium chromate. In the latter case, the intensity of mixed metal ions was more important. $BaCrO_4^-$, $BaCrO_5^-$, $BaCr_2O_7^-$, and $BaCr_2O_8^-$ ions were observed on the negative ion spectrum of barium chromate [Fig. 7(b)]. For magnesium chromate, $MgCr_2O_7^-$ ion was observed [Fig. 7(a)]. The formation of these ions could be the result of aggregation processes between ionic chromium species and neutral MO species (M = Mg or Ba). Pure oxygenated alkaline earth anions—in particular MO—were actually never observed on the two chromate negative ion fingerprints [Figs. 7(a) and 7(b)].

As opposed to what was observed when examining alkali chromate negative ions, the behavior of pure oxygenated chromium cluster ion was identical to that of magnesium, calcium, strontium, and barium chromate compounds. The profile was not modified when considering the $Cr_2O_y^-$ series. It appeared that the most intense ion was always $Cr_2O_5^-$, whatever the alkaline earth chromate counter ion.

3.5.2. FTICRMS studies

The development observed when studying alkali chromate, as experiments were carried out successively with TOF-LMMS and FTICRMS equipment, also appeared when investigating the alkaline earth chromate. The intensity of CrO_2^- cluster ions decreased rapidly in FTICR analysis (Fig. 8); at the same time, $Cr_2O_6^-$ cluster ions displayed highest intensity in the $Cr_2O_y^-$ series.

Again, the difference in stability between CrO_2^- and CrO_3^- ionic structures may be mentioned to account for the preferential formation of the CrO_3^- ion [55].

However, more important modifications occurred when the magnesium [Figs. 7(a) and 8(a)] and barium chromate [Figs. 7(b) and 8(b)] compounds were successively analyzed applying the two techniques. First, we note the disappearance of the mixed metal oxygenated anions on the FTICRMS fingerprint of barium chromate. The poor stability of these anionic structures may account for this observation. Second, we notice a significant increase in the number of cluster anions on the FTICRMS fingerprint of magnesium chromate, as compared to the TOF LMMS one. Moreover, the relative intensity of pure chromium oxygenated cluster ions ($Cr_xO_y^-$) was higher than what was observed on the mass spectra obtained for other FTICR alkaline earth chromate compounds, where only the CrO_3^- ion has some significance.

In fact, the difference in electronegativity between, on the one hand, magnesium and oxygen and, on the

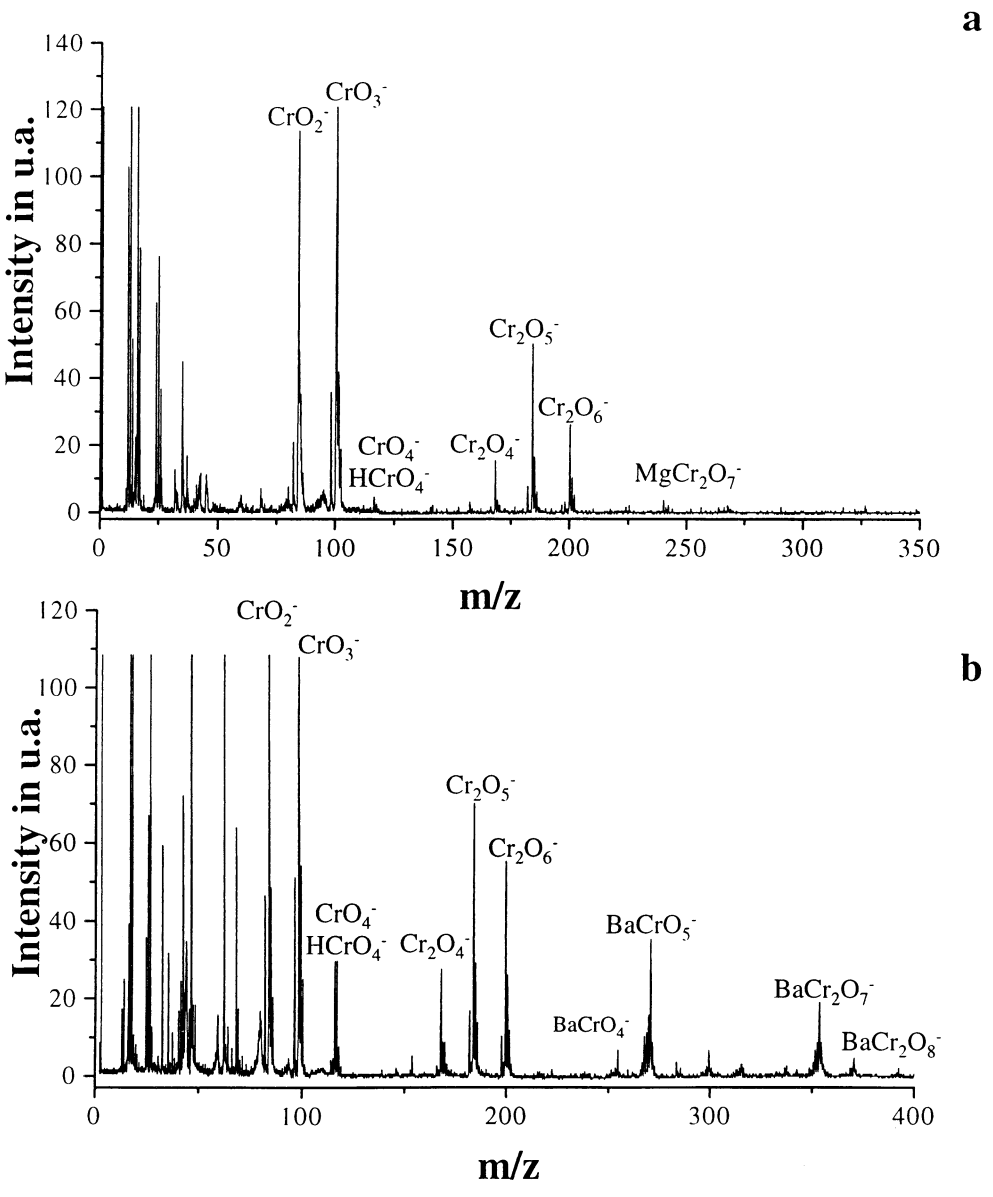

Fig. 7. Negative TOF-LMMS fingerprints (a) $MgCrO_4$ and (b) $BaCrO_4$ at a wavelength of 357.87 nm, with a power density of 3×10^7 W/cm^2.

other hand, chromium and oxygen, and the respective oxygen affinity of the two metal atoms—being very close—could account for this behavior. More chromium oxygen species are produced during laser ablation of magnesium chromate, and less neutral and ionic magnesium species occur in the aggregation process observable in the positive detection mode. In the same time, in the negative detection mode, the larger part of the pure oxygenated chromium species in the plume induced an increase, first in the number of oxygenated chromium cluster anions, and second in their intensity.

The general trend observed for the evolution of the alkali chromate fingerprint may be mentioned to account for what is observed on the fingerprint of alkaline earth chromate when the magnesium, cal-

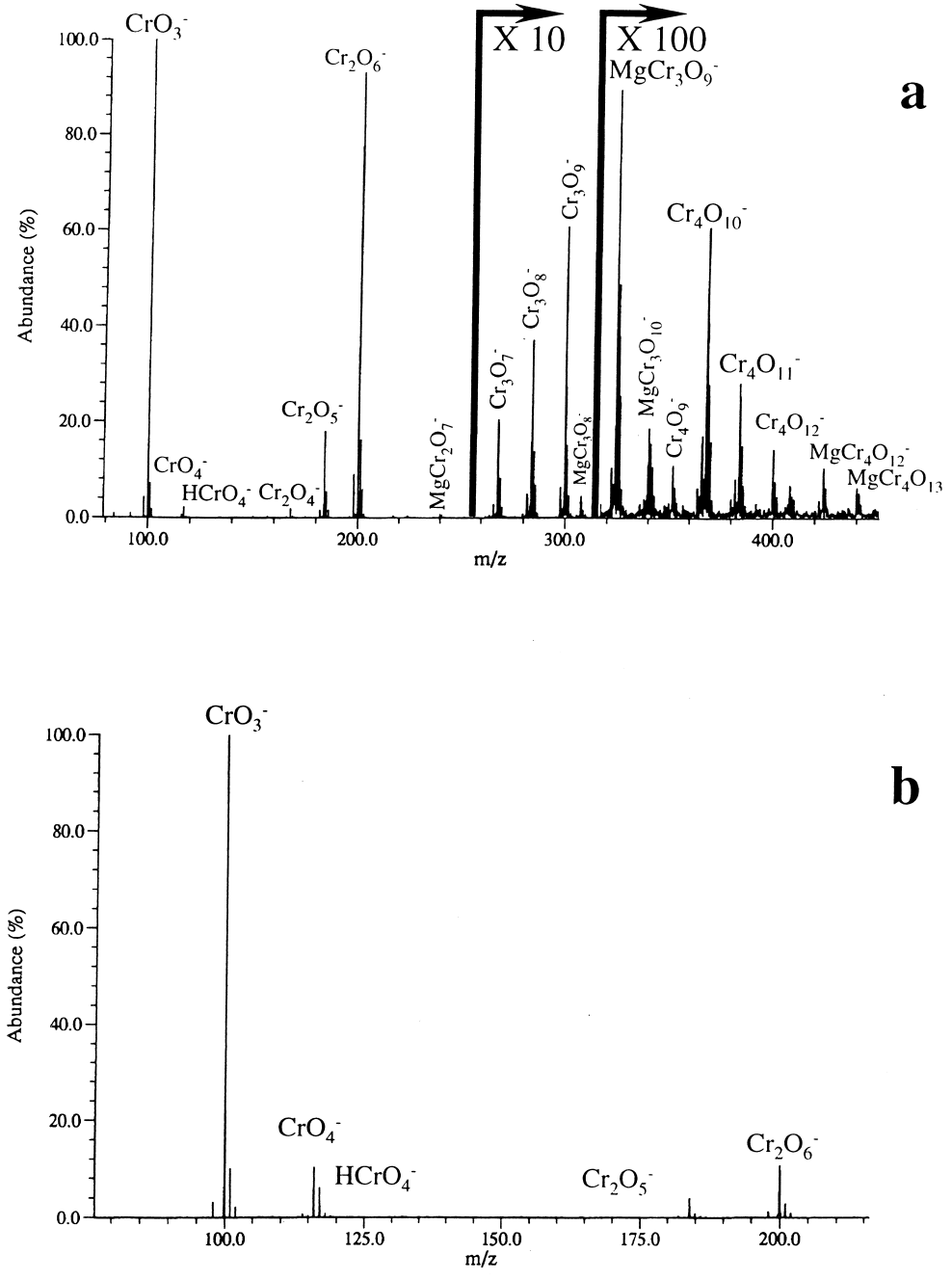

Fig. 8. Negative LA-FTICRMS of (a) $MgCrO_4$ and (b) $BaCrO_4$ at a wavelength of 355 nm, with a power density in the 10^7–10^8 W/cm^2 range.

cium, strontium, and barium compounds were studied successively by mass spectrometry.

The affinity of alkali (respectively, alkaline earth) atoms with oxygen increases with their radius (Table 1). The number of oxygenated alkali (respectively, oxygenated alkaline earth) species versus that of chromium increases. Being less abundant, the latter have lesser importance in the various aggregation

processes. On the one hand, we could observe first a decrease in the number of cluster ions in the negative detection mode and, on the other hand, a decrease, in the positive detection mode, of mixed metal ions with more than one chromium atom in their structure. Finally, we could see an increase in the intensity of the structure of single chromium mixed metal ions whose stability increases with the radius of the counter ion. The progressive growth in cluster ion stability from $Mg_2CrO_4^+$ to $Ba_2CrO_4^+$ is enhanced by the increase in intensity on the LA-FTICR mass spectra; this may be assigned to a corresponding increase in binding energy or to the ionicity of the metal oxygen bond with increasing cation radius (increase of the metal polarizability) [62].

4. Conclusion

Experiments carried out with the TOF-LMMS and the FTICRMS laser microprobe allow us to distinguish alkali and alkaline earth chromate compounds by a detection of specific cluster ions.

The fingerprint obtained for these two sets of compounds by the two laser ablation/ionization mass spectrometry techniques betray similar behavior, first for alkali chromate compounds, second for alkaline earth ones. These two patterns are characteristic of the chromate counter ion. If the latter is an alkali atom, the major cations observed correspond to the general formula $(MO)_nCr^+$ and $(MO)_nCrO^+$ ($n = 2$ or 3), whereas, in the case of alkaline earth atom, the main positive cluster ions are $(MO)_nCrO^+$ and $(MO)_nCrO_2^+$ ($n = 1$–4). This difference may be attributed to the lower oxygen–metal (chromium and alkali or alkaline earth) ratio in the alkali chromate compounds and to the higher oxygen affinity of alkali, as compared to that of alkaline earth in the same row of the periodic table of elements. In general terms, more chromium atoms are available in the laser plume and more oxygenated chromium species are formed in the case of laser ablation of alkaline earth chromate. A similar behavior is observed in the TOF-LMMS fingerprints of alkali chloride and alkaline earth chloride [63,64]. More chlorided cluster ions are formed when analyzing the latter ones.

These results are very important in various respects. First, they might allow for an identification of these compounds in complex samples such as dust particles by a rapid investigation using laser ablation/ionization mass spectrometry. Second, the systematic study of alkali and alkaline earth chromate compounds allows us to gain a better understanding of cluster ion formation processes in the two detection modes. It appeared that there is indeed a clear separation between the information obtained under the positive detection mode and that supplied when using the negative detection mode. Whereas cluster metal anions are mainly pure chromium oxygenated ions and provide information about the species of chromium in the laser plume, cluster metals cations—mostly mixed metal cluster cations—provide information about the nature of the alkali or alkaline earth species produced after the laser ablation.

When the radius increases, the development of the fingerprint induces an exacerbation of the specific behavior of the two types of compounds (alkali or alkaline earth chromate) and, consequently, to enhance the various processes occurring in the laser plume.

This article offers some prior elements for a better understanding of the process of cluster ion formation, but they are rather insufficient to establish with a satisfactory degree of accuracy the various processes occurring in the gaseous cloud above the surface after laser irradiation. The development of the fingerprint with the increasing size of the counter ion radius in the two alkali and alkaline earth series depends closely first on the affinity of counter ion oxygen and second on its polarizability. In fact, these two physical parameters have a great importance in the process of cluster ion formation. On the one hand, a greater affinity of oxygen induces a greater yield of neutral alkali or alkaline earth oxygenated species during the laser ablation process. On the other hand, greater counter ion polarizability induces an increase of the dipole moment of alkali and alkaline earth oxygenated species. The affinity of positively charged chromium increases with the polarizability of the chromate

counter ion, i.e. with its radius. The influence of the production of alkali and alkali earth oxygenated species and their physical properties on the fingerprint obtained seems to be revealing of their leading part in the mixed metal oxygenated cluster ion.

This is the reason why, in the second part of the present study, we intend to investigate the development of the fingerprints obtained with the various compounds by varying several parameters (power density, wavelength, hydration degree). The understanding of the ion formation processes is of prime importance for the analysis of industrial samples to reduce the risk of error. This will be amply discussed in Part II of the present study.

Acknowledgements

The authors gratefully acknowledge financial support from Ugine Savoie. They thank Gabriel Krier, Lionel Vernex Losel for their fruitful technical support, and Benoît Courrier for his TOF-L77S contribution.

References

[1] M. Cieslak-Golonka, Polyhedron 15 (1995) 3667.
[2] K.E. Wetterhahn, E.J. Dudek, New J. Chem. 20 (1996) 199.
[3] K.W. Jennette, Biol. Trace Element Res. 1 (1979) 55.
[4] M.J. Gonzalez Alvarez, M.E. Diaz Garcia, A. Sanz-Medel, Talanta 36 (1989) 919.
[5] J.L. Manzoori, M.H. Sorouaddin, F. Shemiran, Anal. Lett. 29 (1996) 2007.
[6] V. Ososkov, B. Kebbekus, D. Chesbro, Anal. Lett. 29 (1996) 1829.
[7] C.G. Bruhn, L. Villablanca, V.H. Campos, S. Basualto, J. Tapia, Bol. Soc. Chil. Quím. 42 (1997) 83.
[8] S.S.M. Hassan, M.N. Abbas, G.A.E. Moustafa, Talanta 23 (1996) 797.
[9] E. Magalhaes de Souza, A. de Luca, R. Wagener, P. Farias, Croat. Chem. Acta 70 (1997) 259.
[10] I. Turyan, D. Mandler, Anal. Chem. 69 (1997) 894.
[11] H. Schaller, R. Neeb, Z. Fresenius, Anal. Chem. 327 (1987) 170.
[12] J.W. Olesik, J.A. Kinzer, S.V. Olesik, Anal. Chem. 67 (1995) 1.
[13] A.R. Timerbaev, O.P. Semenova, W. Buchberger, G.K. Bonn, J. Fresenius, Anal. Chem. 354 (1996) 414.
[14] M. Panstar-Kallio, P.K.G. Manninen, J. Chromatogr. A 750 (1996) 89.
[15] M.J. Powell, D.W. Boomer, D.R. Wiederin, Anal. Chem. 67 (1995) 2474.
[16] C.M. Andrle, N. Jakubowski, J.A.C. Broeckaert, Spectrochim. Acta B 52 (1997) 189.
[17] M. Sperling, S. Xu, B. Welz, Anal. Chem. 64 (1992) 3101.
[18] J. Posta, H. Berndt, S.K. Luo, G. Schaldach, Anal. Chem. 65 (1993) 2590.
[19] M.S. Jiménez, L. Martín, J.M. Mir, J.R. Castillo, At. Spectrosc. 17 (1996) 201.
[20] A. Hachimi, E. Poitevin, G. Krier, J.F. Muller, J. Pironon, F. Klein, Analusis 21 (1993) 77.
[21] B.M. Weckhuysen, I.E. Wachs, J. Chem. Soc., Faraday Trans. 92 (1996) 1969.
[22] G.P. Huffman, F.E. Huggins, N. Shah, J. Zhao, Fuel Process. Technol. 39 (1994) 47.
[23] S. Bajt, S.B. Clark, S.R. Sutton, M.L. Rivers, J.V. Smith, Anal. Chem. 65 (1993) 1800.
[24] I. Nakai, C. Numako, S. Hayakawa, A. Tsuchiyama, J. Trace Microprobe Tech. 16 (1998) 87.
[25] I. Arcon, B. Mirtic, A. Kodre, J. Am. Ceram. Soc. 81 (1998) 222.
[26] L. Van Vaeck, H. Struyf, W. Van Roy, F. Adams, Mass Spectrom. Rev. 13 (1994) 189.
[27] L. Van Vaeck, H. Struyf, W. Van Roy, F. Adams, Mass Spectrom. Rev. 13 (1994) 209.
[28] B. Maunit, A. Hachimi, P.J. Calba, G. Krier, J.F. Muller, Rapid Commun. Mass Spectrom. 9 (1995) 225.
[29] B. Maunit, A. Hachimi, P. Manuelli, P.J. Calba, J.F. Muller, Int. J. Mass Spectrom. Ion Processes 156 (1996) 173.
[30] T.M. Allen, D.Z. Bezabeh, C.H. Smith, E.M. McCauley, A.D. Jones, D.P.Y. Chang, I.M. Kennedy, P.B. Kelley, Anal. Chem. 68 (1996) 4052.
[31] E. Michiels, R. Gijbels, Spectrochim. Acta B 38 (10) (1983) 1347.
[32] N. Lobstein, E. Million, A. Hachimi, J.F. Muller, M. Alnot, J.J. Ehrhardt, Appl. Surf. Sci. 88 (1995) 307.
[33] N. Chaoui, A. Hachimi, E. Million, J.F. Muller, Analusis 24 (1996) 146.
[34] C.J. Cassady, D.A. Weil, S.W. McElvany, J. Chem. Phys. 96 (1992) 691.
[35] C. Colin, G. Krier, H. Jolibois, A. Hachimi, J.F. Muller, A. Chambaudet, Appl. Surf. Sci. 125 (1998) 29.
[36] K. Poels, L. Van Vaeck, R. Gijbels, Anal. Chem. 70 (1998) 504.
[37] H. Struyf, L. Van Vaeck, K. Poels, R. Van Grieken, J. Am. Soc. Mass Spectrom. 9 (1998) 482.
[38] L. Van Vaeck, A. Adrians, F. Adams, Spectrochim. Acta B 53 (1998) 367.
[39] K.R. Neubauer, M.V. Johnston, A.S. Wexler, Int. J. Mass Spectrom. Ion Processes 151 (1995) 77.
[40] I.I. Stewart, G. Horlick, J. Anal. At. Spectrom. 11 (1996) 1203.
[41] A.B. Gwizdala III, S.K. Johnson, S. Mollah, R.S. Houk, J. Anal. At. Spectrom. 12 (1997) 503.
[42] C. Plog, L. Wiedmann, A. Benninghoeven, Surf. Sci. 67 (1977) 565.

[43] E. Poitevin, J.F. Muller, F. Klein, O. Déchelette, Analusis 17 (1989) P47.
[44] E. Poitevin, G. Krier, J.F. Muller, R. Kaufmann, Analusis 20 (1992) M36.
[45] A. Hachimi, E. Poitevin, G. Krier, J.F. Muller, J. Pironon, F. Klein, Analusis 21 (1993) 77.
[46] F. Aubriet, B. Maunit, B. Courier, J.F. Muller, Rapid Commun. Mass Spectrom. 11 (1997) 1596.
[47] G. Henrich, Z. Electrochem. 58 (1954) 183.
[48] R.G. Darrie, W.P. Doyle, I. Kirkpatrick, J. Inorg. Nucl. Chem. 29 (1967) 979.
[49] B. Authenrieth, Berichte der deutschen chemischen Gesellschaft 34 (1904) 3882.
[50] F. Schröder, Ann. Chem. 174 (1874) 249.
[51] G. Krier, F. Verdun, J.F. Muller, Fresenius Z. Anal. Chem. 322 (1985) 379.
[52] F.R. Verdun, G. Krier, J.F. Muller, Anal. Chem. 59 (1987) 1383.
[53] J.F. Muller, M. Pelletier, G. Krier, D. Weil, J. Campana, Microbeam Analysis, P.E. Russell (Ed.), San Francisco Press Inc., San Francisco, 1989, p. 311.
[54] M. Pelletier, G. Krier, J.F. Muller, D. Weil, M. Johnston, Rapid Commun. Mass Spectrom. 2 (1988) 146.
[55] A. Hachimi, E. Poitevin, G. Krier, J.F. Muller, M.F. Ruiz-Lopez, Int. J. Mass Spectrom. Ion Processes 144 (1995) 23.
[56] A. Marshall, F.R. Verdun, Fourier Transforms in NMR, Optical, and Mass Spectrometry, Elsevier, Amsterdam, 1990.
[57] B. Jöst, B. Schueler, F.R. Krueger, Z. Naturforsch. 37a (1982) 18.
[58] G. Wan, R.B. Cole, Anal. Chem. 70 (1998) 873.
[59] Nouveau Traité de Chimie Minérale, Tome XIV, Masson, Paris, 1957.
[60] W.A. Saunders, Phys. Rev. 37 (1988) 6583.
[61] A. Mele, D. Consalvo, D. Stranges, A. Giardini-Guidoni, R. Teghil, Int. J. Mass Spectrom. Ion Processes 95 (1990) 359.
[62] W.R. Ferrell, M.J. Van Stipdonk, E.A. Schweikert, Nucl. Instrum. Methods Phys. Res. B 112 (1996) 55.
[63] J.F. Muller, A. Ricard, M. Ricard, Int. J. Mass Spectrom. Ion Processes 62 (1984) 125.
[64] J. Dennemont, J.C. Landry, Microbeam Analysis, J.T. Armstrong (Ed.), San Francisco Press Inc., San Francisco, 1985, p. 305.
[65] A.M. Jones, M.P. Lord, Macmillan's Chemical and Physical Data, Macmillan, London, UK, 1992.
[66] J.E. Huhcey, E.A. Keiter, R.L. Keiter, Inorganic Chemistry: Principles of Structure and Reactivity, 4th ed., Harper Collins, New York, 1993.
[67] M.W. Chase, Jr., J. Phys. Chem. Ref. Data, Monograph 9, 1998 1.
[68] T.M. Miller, B. Bederson, Adv. At. Mol. Phys. 13 (1977) 1.